ICAS-88-2.1.3

HEAT TRANSFER MEASUREMENTS ON BICONICS AT INCIDENCE IN HYPERSONIC HIGH ENTHALPY AIR & NITROGEN FLOWS

S.L. Gai
Dept.of Mech.Eng'g., University College,U.N.S.W., Australian Defence Force Academy
Canberra, A.C.T.,2600, Australia.

T. Cain, W.S. Joe & R.J. Sandeman
Dept.of Physics & Theoretical Physics, The Australian National University,
Canberra, A.C.T.,2601, Australia.

C.G. Miller
Experimental Aerodynamics Branch, Space Systems Division,
NASA Langley Research Center, Hampton, Va., U.S.A.

Abstract

This paper reports measurements of heat transfer rates on a $12.84^{o}/7^{o}$ straight biconic which is a 1.9 per cent scale model of an aeroassisted orbital vehicle proposed for missions to a number of planets. Measurements were obtained with the model set at angles of attack of 0^{o},5^{o},15^{o} and 21^{o}. Comparison with low enthalpy data by Miller et al[5] showed a limited correlation with the windward data. The windward heat transfer correlations were based on equilibrium flow in the shock layer of the model although it is possible that the flow may depart from equilibrium in the flow field. No correlation of the leeward data has been attempted because of the uncertainty of the establishment of separated flow on the leeward side at angles of attack. Similar uncertainty in regard to leeward flow existed in Miller et al's data[5] also. All the experiments were conducted in the Australian National University Free-Piston Shock Tunnel T3. Heat transfer distributions were measured using palladium thin-film resistance gauges deposited on MACOR glass ceramic substrate.

I. Introduction

There has been a resurgence of interest in the study of aero-thermodynamic problems of hypervelocity flight with the proposed plans for building aero-assisted orbital transfer vehicles (AOTVs). These new generation of spacecraft will be subject to prolonged radiative and convective heating during their trajectory through low density upper atmosphere at speeds ranging from 10 km/s to 5 km/s. It is important, therefore, to understand the physical and chemical gas dynamic processes in the flow over such vehicle configurations. One such is the 'on-axis' biconic configuration shown in Figure 1.

A comprehensive data base on biconics, both on-axis and bent nose, have been built up by the NASA Langley Research centre in recent years.[1,2,3,4,5] This includes both computational and experimental studies of aerodynamic coefficients, pressure distributions, shock shapes and heating rates. The experimental studies have been carried out in conventional hypersonic wind tunnels and the Langley Expansion tube[6] which simulates hypervelocity real gas flows but whose capability is still not sufficient to simulate re-entry flight conditions of AOTVs. The ANU Shock Tunnel T3, on the other hand, is capable of producing flows at much higher enthalpies than any other facility currently available and as such is better able to simulate AOTV re-entry speeds and temperatures (see Fig.2).

The paper presents measurements of heat transfer rates on a $12.84^{o}/7^{o}$ straight biconic model as tested in the ANU T3 Shock Tunnel at stagnation enthalpies of 26 MJ/kg or an equivalent flight speed of 7.2 km/s. Both air and nitrogen were used as test gases. The model was tested at angles of attack, 0^{o},5^{o},15^{o} and 21^{o} and heat transfer measurements were taken on both windside and leeside of the model. The basic aim of the work is to establish the heat transfer data base to higher enthalpies unavailable at present.

II. Facility, Model and Instrumentation

Facility. The ANU T3 Shock Tunnel was used in the present experiments in the reflected mode. In this mode of operation the reservoir of test gas created by the passage of an incident and a reflected shock, undergoes an unsteady expansion in the shock tube prior to its steady expansion in a hypersonic nozzle. The reflected mode of operation has the beneficial effect of increasing the uncontaminated test time by drawing back the driver gas from the nozzle entrance. The method results in a drop in stagnation pressure when the reflected shock encounters the driver gas but, after a short interval, when the reflected shock has been attenuated by the following unsteady expansion, a plateau is reached in the stagnation pressure which provides a steady flow test time. The driver gas (Helium) volumetric compression ratio, which is a fundamental operating parameter, was maintained at 60 which has been found to give sufficient period of uncontaminated steady flow and the variation of stagnation enthalpy is achieved simply by varying the initial shock tube pressure.

A conical nozzle of 7.5^{o} half angle with exit and throat diameters of 305 mm and 12.7 mm was used to generate the free stream. The model was placed off-axis in the 200 mm inviscid core with its nose just upstream (-40 mm) or downstream (+10 mm) of the nozzle exit plane, depending on incidence.

Model. The model used is a 'straight' or 'on-axis' biconic which is a 1.9 per cent scale model of a proposed aero-assisted orbital transfer vehicle (Fig.1). The model is made of stainless steel except for the nose which is made of MACOR, a machinable glass ceramic. On its body five slots are machined to locate instrumented inserts each of which consists of eight thin film resistance gauges deposited on the MACOR substrate. The thin

film gauges and the associated constant current supplies were made and supplied by NASA, Langley workshops.

Instrumentation. The thin film resistance gauges are made of palladium and are approximately 0.12 μm thick and in the form of a serpentine pattern providing a sensing area of 1.02 mm x 1.27 mm. A coating of acrylic lacquer of about 0.2 μm thick was provided to the gauges to protect them from ionisation effects, especially with air as test gas. Tests were carried out to monitor the temperature of gauges with 0.2 μm coating and a non-coated gauge, placed side by side. These indicated that once the initial layer of ionised gas has passed over, both the gauges yielded the same value of temperature. This indicated that the presence of the coating did not seriously influence the thermal response of the gauge and hence the heat transfer rate.

A constant current of 2 mA was applied to the gauges and the voltages across the gauges were input to high impedance amplifiers. The output from the amplifiers was then recorded on two eight channel Le Croy 2264 transient recorders which sampled each channel every 25 μs (i.e. 400 kHz).

There was no electronic filtering of the signal other than the 100 kHz bandwidth of the impedance matching voltage followers which supplied the transient recorders.

Data were collected from the recorders through an IEEE 488 bus for the Macintosh PC and then numerically processed.

III. Computation of Heat Transfer Rates and Data Accuracy.

Computation of Heat Transfer Rates. All heat transfer rates are calculated by numerical integration of temperature traces on a Macintosh PC using the semi-infinite one dimensional heat transfer model and neglecting gauge and insulation thickness effects. These assumptions lead to the following relation:

$$\dot{q}(n) = \frac{2}{\alpha_R E_o \sqrt{\pi \Delta t}} \sum_{i=1}^{n} \frac{E(i) - E(i-1)}{(n-i)^{\frac{1}{2}} + (n-i+1)^{\frac{1}{2}}} \qquad \ldots(1)$$

(see eqn. 83, Schultz & Jones[8])

where $\dot{q}$ = heat transfer rate (w/m^2),
E_o = voltage across the gauge,
$\beta = (\rho ck)^{\frac{1}{2}}$ = thermal product of the substrate,
and α_R = temperature coefficient of resistance.

The values of α_R and β were obtained by direct calibration and were found to be in excellent agreement with Miller et al[5] data. In particular the values used in the calculations were:
β = 2004 W sec$^{\frac{1}{2}}$/m^{2}K; $\alpha_R = 2.23 \times 10^{-3}$/K.

The calculated heat transfer rates are corrected to account for the variation of thermal properties of MACOR substrate using the relation given by Miller et al[5]:

$$\dot{q} = \dot{q}(n)(1 + 6.38 \times 10^{-4} \Delta T_W) \qquad \ldots(2)$$

Accuracy of the Data. Previous heat transfer studies made in this facility[9] have estimated Stanton number accuracies of better than 20 per cent. This was arrived at from identifying errors in the measurement of stagnation enthalpy (± 10%), stagnation pressure (± 5%) and the recording instrumentation (± 5%). Based on the same criterion, but noting that the present gauges and recording instrumentation are the same as those used by Miller et al[5] albeit some modern data processing, the accuracy of the gauge and recording instrumentation is taken to be nearer ±5% rather than ± 10% assumed by Miller et al[5]. On this basis, the overall accuracy of heat transfer data is expected to vary between 10 to 20 per cent. Error bars of ± 15 per cent have therefore been ascribed to the data.

IV. Test Conditions.

Test conditions are obtained by calculating the nozzle reservoir conditions from the measured shock speed and reservoir pressure, taking the gas to be in thermodynamic equilibrium, and subsequently calculating the non-equilibrium flow through the conical nozzle by the one-dimensional flow method of Lordi, Mates & Moselle[10]. The free stream conditions at the exit of the nozzle obtained in this way are shown in Table 1. Extensive measurements by Stalker et al[11] made in the shock tunnel T3 have confirmed that the calculated free stream velocities and stagnation enthalpies are realised in the test section.

In the present experiments, the flow period in which the steady state heat transfer occurs is between 250 μs to 400 μs after the arrival at the model of the nozzle starting shock. A plateau in stagnation pressure also occurs between 250 μs to 400 μs after shock reflection. A typical stagnation pressure and heat transfer trace are shown in Figure 3.

The conical nozzle flow results in decreasing pitot pressure along the axis and hence along the length of the model. The effect of flow angularity would be expected to have the largest effect at higher angles of attack when the model occupies a greater proportion of the inviscid core. This was thought to result in large variations in measured heat transfer. However, as Fig.4 shows, the variation of pitot pressure within the region of the model locations is less than 8 per cent. The heat transfer variation for a stagnation point on a sphere in the same region is less than 4 per cent. It is, therefore, assumed that effects of conicity of the nozzle on heat transfer date have not been serious.

V. Results and Discussion.

Windward Data. Figures 5 and 6 show the heat transfer data presented in terms of the ratio $(\dot{q}/\dot{q}_{sph})$ where $\dot{q}_{sph}$ is the heat transfer rate at the stagnation point of a sphere whose radius is equal to the nose radius of the biconic. $\dot{q}_{sph}$ was calculated from the empirical expression

$$\dot{q}_{sph} = K\left(\frac{P_{t_2}}{r_n}\right)^{\frac{1}{2}} (h_{t_2} - h_w) \qquad \ldots(3)$$

where P_{t_2} (atm) is the stagnation pressure behind the bowshock at the spherical nose;
h_{t_2} (MJ/kg) is the corresponding stagnation enthalpy;
h_w (MJ/kg) is the wall enthalpy;
r_n (m) is the spherical nose radius.

The proportionality constant K varies depending on the test gas. It is 0.1113 $kgs^{-1}m^{-3/2}atm^{-\frac{1}{2}}$ for air and 0.112 $kgs^{-1}m^{-3/2}atm^{-\frac{1}{2}}$ for nitrogen. Expression (3) has been used by Miller et al[5] and was originally proposed by Sutton and Graves[12] for equilibrium stagnation point convective heat transfer rate to a sphere in a medium of arbitrary gas mixtures.

In applying eqn.(3) in the present case, certain simplifying assumptions have been made. Firstly, in the shock layer at the nose behind the bow shock, we have taken the recovery enthalpy h_r as approximately the same as the free stream stagnation enthalpy h_s. This, of course, assumes equilibrium flow in the shock layer. In reality, it is possible that a significant proportion of the free stream enthalpy is locked up as frozen chemical enthalpy. If, after passing through the bow shock, the flow remains frozen, then $h_r < h_{t_2} (=h_s)$ and the value of q_{sph} as obtained from eqn.(3) would be an overestimate.

We note from Figures 5 and 6 that the present data and the low enthalpy (≈16 MJ.kg) NASA data[5] correlate reasonably well especially at higher angles of attack. The correlations are particularly better on the aft cone.

An equally good correlation is obtained if we use $\left(\frac{St\sqrt{Re_L}}{Sin\theta_{eff}}\right)$ as a correlating parameter. Figures 7 and 8 show these results. Here Re_L is the Reynolds number based on free stream mass flow per unit area and viscosity based on conditions behind the bow shock. Such a Reynolds number has been used to correlate stagnation point heat transfer rates. This Reynolds number is used because, to a first approximation, the flow downstream of a hypersonic bow shock wave is independent of the temperature (hence viscosity) ahead of it. This means that any necessity of quoting the free stream Reynolds number of the tunnel is eliminated as this can vary widely without substantially affecting the Reynolds number of the flow over the body. Again, inclusion of $Sin\theta_{eff}$ term takes into account the angle of attack effects.[5] St is the Stanton number based on freestream mass flow per unit area and the stagnation enthalpy $(=\dot{q}/\rho_\infty v_\infty (h_s - h_w)$.

Leeward Data. Leeward heat transfer rates for angles of attack ranging from 5° to 21° were measured during the experiments but only 15° and 21° results are presented here as these give some indication as to the behaviour of separated flow on the leeward side at these angles of attack. Miller et al[5] have shown, from detailed experimental data from a continuous hypersonic tunnel, that the flow on the leeside of a straight biconic is separated when the fore cone angle of attack (α) is greater than the fore cone half angle (θ_c). Stetson[13] suggests a criterion for incipient separation which is $\frac{\alpha}{\theta_c} \approx 0.7$ for a cone at angle of attack in hypersonic flow. On this basis, in the present instance, the incipient separation would occur at about 10°. Thus, tests with 15° and 21° incidence should give an indication of the nature of the separated flow on the leeside.

It must be stressed, however, that it is not completely certain that the leeside flow is at all established during the few hundred microseconds of uncontaminated steady flow of the shock tunnel. Another reason for the uncertainty in leeside test data is the low output signals compared to the electrical noise. For these reasons, the leeside data should only be considered as indicative at best.

Figure 9 shows measured heating rates on the most windward and leeward sides for nitrogen. These results show that the fore cone windward heating rates are about 8 to 10 times the leeward heating rates for both angles of attack. These core results are similar to those of Miller et al[5]. On the aft cone, while the 21° angle of attack windward heating rates are about 4.5 to 5 times the leeward heating rates, the 15° angle of attack results show that windward and leeward data are much closer. The air results too showed similar trend.

The probable reasons for the difference in the 15° and 21° leeside results are the nature of the vortices and leeside flow separation. With the moderate angle of attack (15°), the two counter-rotating longitudinal helical vortices emanating from the nose region[13], being close to the surface, interact with the shear layer and a vortex break-down may occur. The effect of vortex break-down is an increase in the size of the vortex cores resulting in a stronger mutual interaction as well as interaction with the flow near the surface. This presumably results in higher heat transfer.

When the angle of attack is sufficiently large, as at 21°, the vortices are generated further upstream near the nose and are not as close to the surface on the aft cone so that their interaction with the separated shear layer is weak and the vortex break-down may not occur, thus resulting in lower heat transfers.

Effects of Non-Equilibrium. In a reflected shock tunnel, the free-stream is produced by a steady expansion of the test gas in a hypersonic nozzle from a reservoir in thermodynamic equilibrium. However, for sufficiently high enthalpies the nozzle freezing phenomenon results in a free stream which is not in equilibrium. In the present instance, the free stream consists of (almost all) dissociated oxygen and some atomic nitrogen. This results in a decrease in free stream velocity due to the chemically absorbed energy and an increase in the value of γ due to increase in the number of particles with only translational degrees of freedom. This has an influence on the density ratio across the shock and the post shock flow in the shock layer of the body.

In presenting the data above, we have assumed that the recovery enthalpy h_r is approximately the same as the free stream stagnation enthalpy. This, of course, assumes equilibrium in the shock layer. In reality, it is possible that a significant proportion of the free stream enthalpy is still locked up as frozen chemical enthalpy. Thus, if after passage through the bow shock, the flow remains frozen, then $h_r < h_s$ and the shock layer flow will be in non-equilibrium.

To throw some light on this situation, heat transfer data was obtained at stagnation enthalpies which were nominally close to those of

Miller et al[5] and was compared with their data assuming non-equilibrium in the shock layer and using recovery enthalpy h_r instead of h_s. In other words, including the effects of frozen chemistry. Figure 10 shows the results with air as test gas. This shows some interesting features. The fore cone data seem to agree very well suggesting flow non-equilibrium possibly exists both in the present case as well as in Miller et al[5]. The aft cone data seem consistent with equilibrium type of flow. In Fig.10 the heat transfer data are presented in terms of $(St(\rho_2/\rho_\infty)^{\frac{1}{4}}/\bar{V}^*\sin\theta_{eff})$ because normal shock density ratios in the two cases are different. Here St is the Stanton number $(=q/\rho_\infty V_\infty(h_s - h_w))$, ρ_2/ρ_∞ the normal shock density ratio and $\bar{V}^*(= M_\infty\sqrt{C^*/Re_{\infty L}})$ is the rarefaction parameter. The inference from these results would suggest that the flow in the shock layer of the fore-body is likely to be in non-equilibrium. Although in making comparisons like shown in Fig.10 the nominal stagnation enthalpies in the present tests and Ref.5 are not far different, other flow properties such as free stream density, temperature, velocity and Mach number are very much different. It is, therefore, likely that some of the differences observed in the two sets of data are to some extent attributable to these differences although it is difficult to single out the effect of each of them on the data.

Non-equilibrium in the Boundary Layer. If the characteristic time (t_r) required for atom recombination is much smaller than the time required for atom diffusion across the boundary layer (t_d), then the boundary layer is in equilibrium so that the recombination is completed before the atoms have time to diffuse to the cold surface. This sets an upper limit to the surface heat transfer. For this case, the catalycity of the surface has no influence as regards surface heat transfer. If, on the other hand, the characteristic time t_r is so large that no recombination can occur before the atoms have diffused to the surface, the boundary layer is in a frozen state. This is usually characterised by the Damkohler number Dg which is the ratio t_d/t_r so that

$Dg \to \infty$ (equilibrium)

$Dg \to 0$ (frozen).

In the case of a partially or completely frozen boundary layer, catalycity of the surface can be important in regard to surface heating. Thus, for a fully catalytic surface, all atoms that diffuse to the surface can recombine there, releasing their chemical energy on the surface and thereby enhancing the heat transfer rate. If the surface is not fully catalytic, the heat transfer rate is reduced because of the slowness or total absence of surface recombination. A completely frozen boundary layer on a fully non catalytic surface, therefore, represents a lower bound on surface heat transfer. Similar to boundary layer Damkohler number Dg, one can define a surface Damkohler number $Ds(= \frac{t_d}{t_s})$ where t_s is the characteristic surface reaction time. Then

$Ds \to \infty$ - fully catalytic

$Ds \to 0$ - fully non-catalytic.

Glossy materials such as pyrex, quartz generally exhibit non-catalytic behaviour while metallic surfaces are generally catalytic.

Attention was, therefore, given to possible surface catalycity effects because of the stainless steel model and MACOR substrate of the gauges. Tests conducted with and without non-catalytic cover (2 μm thick acrylic lacquer coating on the model) showed no change in heat transfer results. The assumption is, therefore, made that the heat transfer data here pertain to a non-catalytic surface.

As a further confirmation, the gas phase Damkohler number in the boundary layer Dg was calculated using the expression given by East et al[9] based on the reaction

$O + O + M \to O_2 + M$ - for air, and

$N + N + M \to N_2 + M$ - for nitrogen

which gave values of Dg of the order of 3.5×10^{-3}, based on the conditions behind the equilibrium bow shock and assuming the velocity at the edge of the boundary layer to be approximately the same as the free stream. This suggested that the boundary layer was frozen. Also, extensive heat transfer study on a flat plate in this facility[11] has shown that surfaces such as aluminium and steel (SiO_2 coated) were non-catalytic under flow conditions similar to these.

VI. Conclusions.

Measurements of heat transfer are described on a $12.84^o/7^o$ straight biconic which is a 1.9 per cent scale model of an aero-assisted orbital transfer vehicle proposed by the NASA for planetary missions.

The primary objective of the present investigation was to establish a heat transfer data base to higher enthalpy flows than has been hitherto possible. Extensive comparisons have been made of the present windward data and that of Miller et al[5] to show that data obtained in two different types of facilities can be correlated.

Some leeward data has been presented but no correlation of this data has been attempted because of the uncertainty of the establishment of separated flow on the leeward side at angles of attack.

Effects of flow non-equilibrium on the data obtained have been discussed and it is shown that the data obtained in equilibrium and non-equilibrium flows could be correlated when non-equilibrium effects are taken into account.

The present data are the first detailed measurements to be obtained under these extreme conditions. By showing that they correlate reasonably adequately with the lower enthalpy data obtained by NASA[5], it is shown that the data base can be extended to higher enthalpies quite reliably.

Acknowledgements. Grateful acknowledgement is made to the Australian Research Grants Scheme for their financial support during the course of this work. Technical assistance of Messrs Ian Darrack and Paul Walsh in operating the T3 facility is also acknowledged.

References

1. Walberg,G.D., "A Survey of Aero-assisted Orbit Transfer", J.of Spacecraft and Rockets, No.1, Vol.22, 1985.

2. Miller,C.G. & Gnoffo,P.A., "Pressure Distributions and Shock Shapes for 12.84°/7° On-axis and Bent-nose Biconics in Air at Mach 6", NASA TM-83-222, Dec. 1981.

3. Miller,C.G., "Experimental and Predicted Heating Distributions for Biconics at Incidence in Air at Mach 10", NASA, Tech.Paper 2334, Nov.1984.

4. Miller,C.G., Blackstock,T.A., Helms,V.T. & Midden,R.E., "An Experimental Investigation of Control Surface Effectiveness and Real Gas Simulation for Biconics", AIAA-83-0213, Jan. 1983.

5. Miller,C.G., Micol,J.R. & Gnoffo,P.A., "Laminar Heat Transfer Distributions on Biconics at Incidence in Hypersonic Hypervelocity Flows", NASA Tech.Paper 2213, Jan. 1985.

6. Graves,R.A. Jr,& Hunt,J.L. "Nasa's Hypersonic Fluid and Thermal Physics Program (Aerothermodynamics)", AIAA-85-0922, June 1985.

7. Stalker,R.J., "Development of Hyper Velocity Wind Tunnel", Aero.J. of Roy.Aero.Soc.,Vol.76, p.374, 1972.

8. Schultz,D.L. & Jones,T.V., "Heat Transfer Measurements in Short Duration Facilities", AGARD Rept.No.165, Feb. 1973.

9. East,R.A., Stalker,R.J.,& Baird,J.P., "Measurements of Heat Transfer to a Flat Plate in a Dissociated High Enthalpy Laminar Air Flow", J.Fluid Mech., Vol.97, Pt.4, p.673, 1980.

10. Lordi,J.A., Mates,R.E., & Mosaelle,J.R., "Computer Program for the Numerical Solution of Non-Equilibrium Expansions of Reacting Gas Mixtures", NASA, Cr-472, 1966.

11. Stalker,R.J., "Free-Piston Shock Tunnel T3 - Facility Hand Book", 1986.

12. Sutton,J., & Graves,R.A., "A General Stagnation Point Convective Heating Equation for Arbitrary Gas Mixtures", NASA TR, R-376, Nov. 1972.

13. Stetson,K.F., "Boundary Layer Separation on Slender Cones at Angle of Attack", AIAA J., Vol.10, No.5, 1972.

Table 1.

(a) Free-stream Conditions at the Exit Plane of the Nozzle.

Test gas	Stagnation enthalpy h_s (MJ/kg)	Stagnation pressure p_0 (atm)	Freestream pressure p_∞ (atm)	Freestream density ρ_∞ (kg/m^3)	Freestream temperature T_∞ (K)	Freestream velocity U_∞ (km/s)	Freestream Mach number M_∞	Freestream Reynolds No Re_∞/m	Rarefaction Parameter $\bar{V}^*$	γ_f
Air	26.36	137	0.00424	1.059×10^{-3}	1137	6.113	8.01	1.45×10^5	0.055	1.473
Nitrogen	26.12	137	0.00365	1.124×10^{-3}	944	5.875	8.57	1.69×10^5	0.053	1.46

(b) Post Normal Shock Flow Conditions (assuming equilibrium).

Test gas	h_{t_2} (MJ/kg)	P_{t_2} (atm)	T_{t_2} (K)	h_w (MJ/kg)	q_{sph} (MW/m^2)	Normal shock density ratio (ρ_2/ρ_∞)
Air	23.36	0.392	9246	0.30	29.25	11.8
Nitrogen	26.12	0.370	9.389	0.31	29.19	11.34

(c) Mole Fractions.

Test gas	N_2	N	E	O_2	O	NO	Ar
Air	0.602	0.052	2.09E-6	2.17E-4	0.337	3.20E-4	7.50E-3
Nitrogen	0.702	0.298	1.64E-5	-	-	-	-

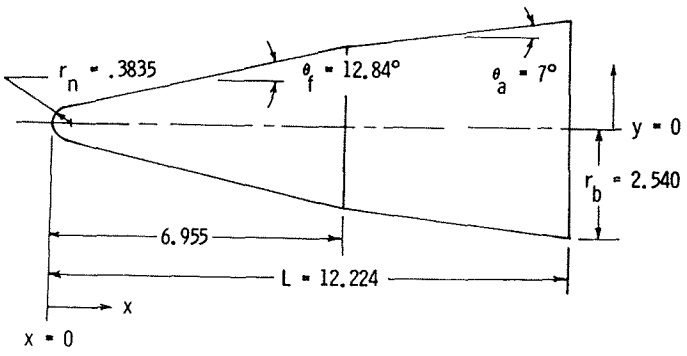

Fig.1 Straight on-axis Biconic Model. Dimensions in cms.

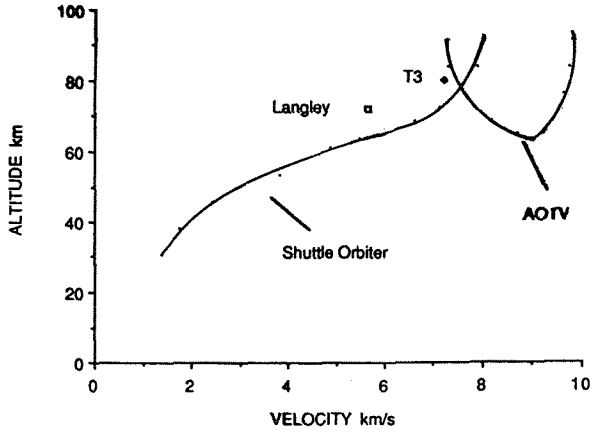

Fig. 2 ANU T3 Shock Tunnel Capability for AOTV simulation.

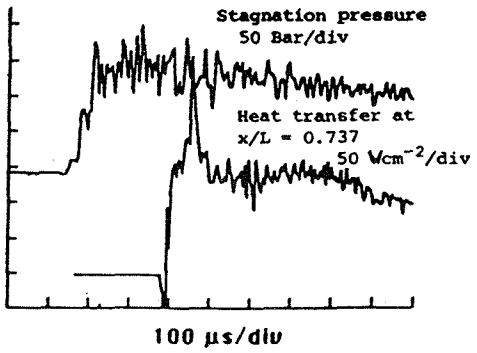

Fig. 3 Typical Stagnation Pressure & Heat Transfer Traces; $\alpha = 5^o$, V_∞ = 6 km/s, Windside.

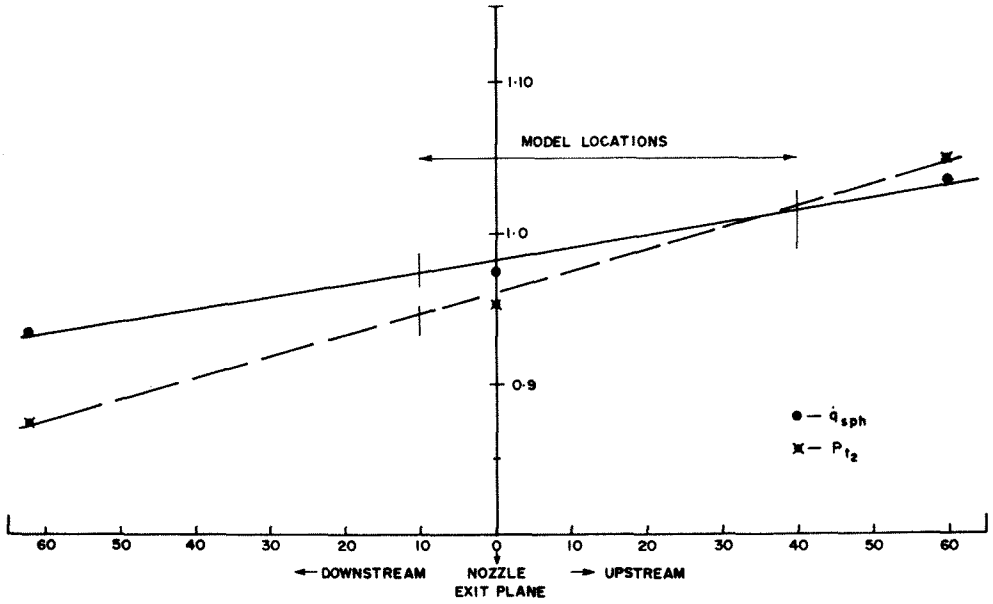

Fig. 4 Variation of Flow properties in the model location region.

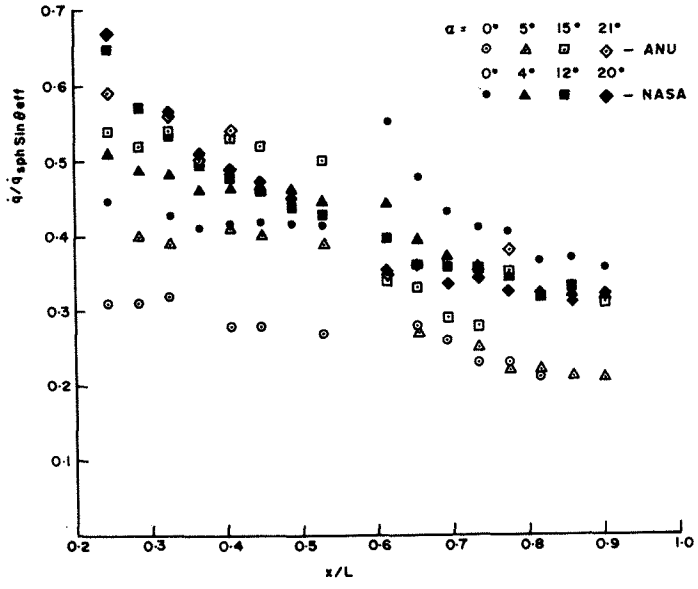

Fig. 5 Windward Data with ($\dot{q}/\dot{q}_{sph}$) as the Correlating Parameter, Air.

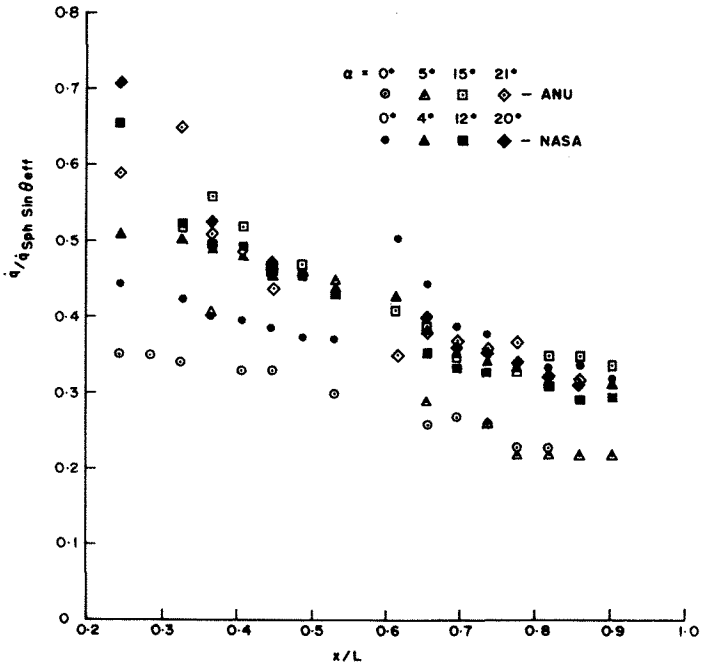

Fig. 6 Windward Data with $(\dot{q}/q_{sph})$ as the Correlating Parameter, N_2.

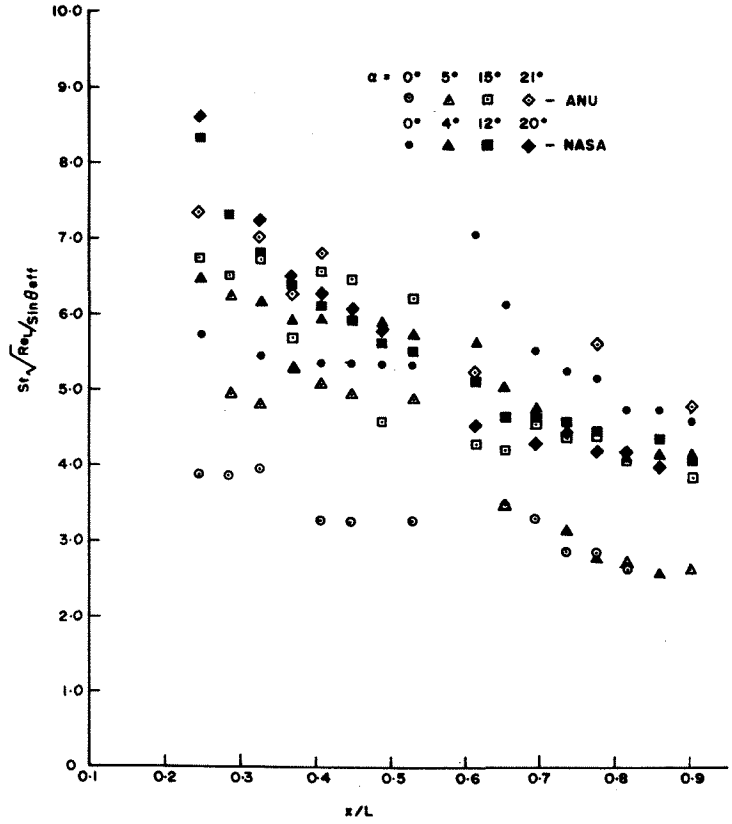

Fig. 7 Windward Data in terms of $\left(\frac{St\sqrt{Re_L}}{Sin\theta_{eff}}\right)$, Air.

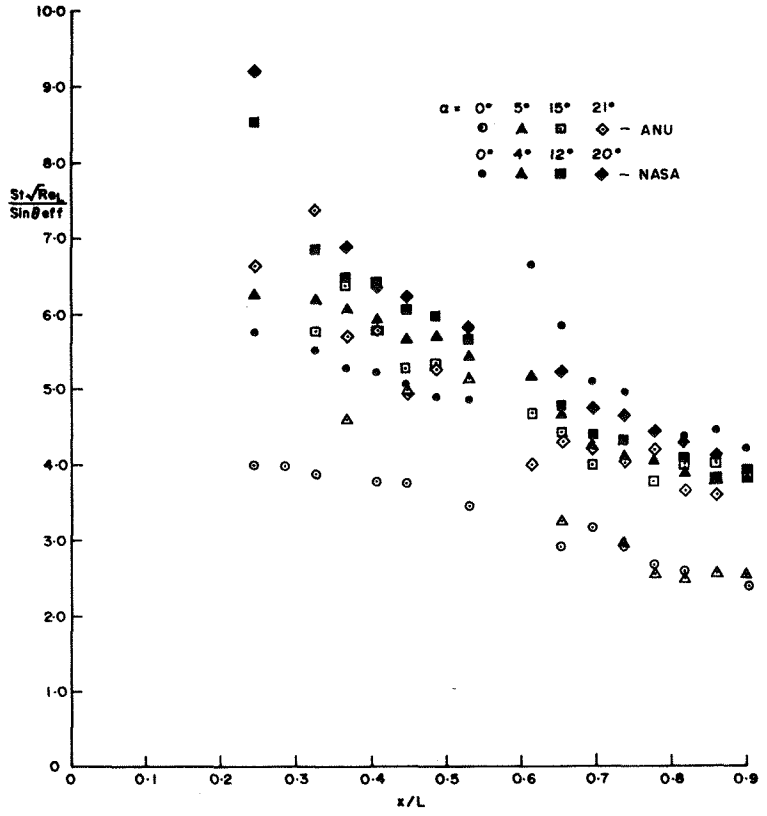

Fig. 8 Windward Data in terms of $\left(\frac{St\sqrt{Re_L}}{Sin\theta_{eff}}\right)$, N_2.

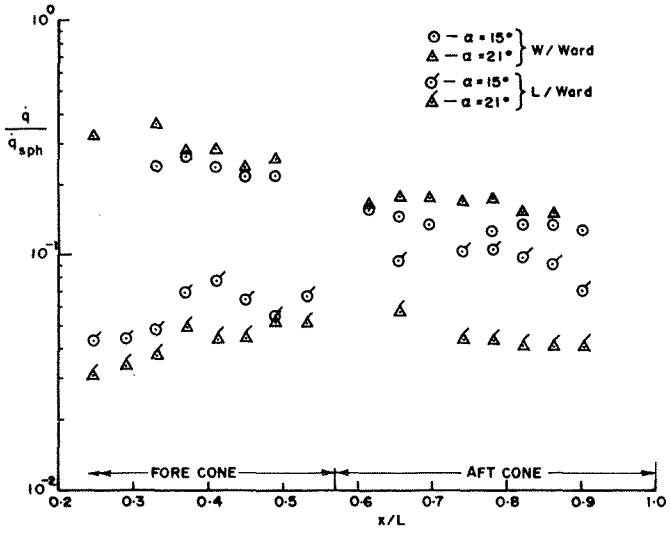

Fig. 9 Leeward Heating Data for Nitrogen.

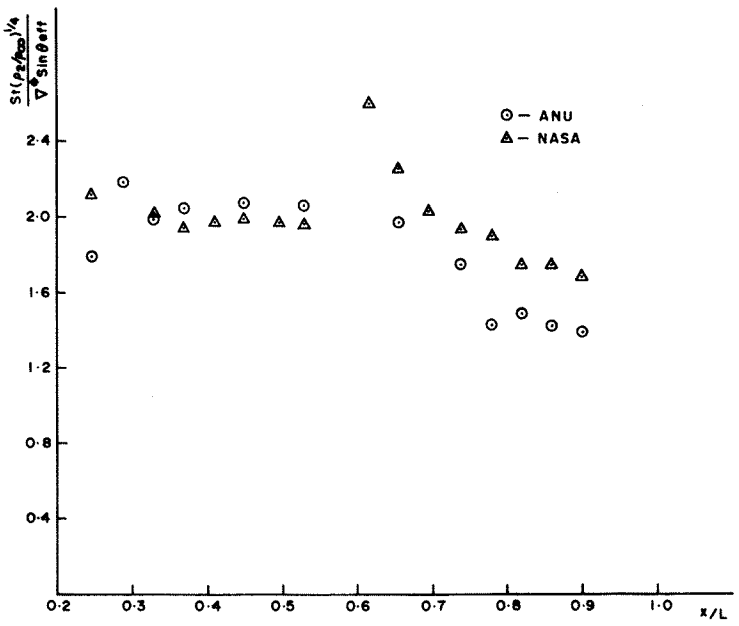

Fig. 10 Heat Transfer Data Showing the Effect of Frozen Chemistry (Air).